Coregulation of extracellular vesicle production and fluconazole susceptibility in Cryptococcus neoformans

Juliana Rizzo, Adèle Trottier, Frédérique Moyrand, Jean-Yves J.-Y. Coppée, Corinne Maufrais, Ana Claudia G. Zimbres, Thi Tuong Vi Dang, Alexandre Alanio, M. Desnos-Ollivier, Isabelle Mouyna, et al.

AMERICAN SOCIETY FOR MICROBIOLOGY | mBio

Check for updates

| Mycology | Research Article

Coregulation of extracellular vesicle production and fluconazole susceptibility in *Cryptococcus neoformans*

Juliana Rizzo,[1,2] Adèle Trottier,[1] Frédérique Moyrand,[1] Jean-Yves Coppée,[1] Corinne Maufrais,[1,3] Ana Claudia G. Zimbres,[2] Thi Tuong Vi Dang,[1] Alexandre Alanio,[4,5] Marie Desnos-Ollivier,[4] Isabelle Mouyna,[1] Gérard Péhau-Arnaude,[6] Pierre-Henri Commere,[7] Sophie Novault,[7] Iuliana V. Ene,[8] Leonardo Nimrichter,[2] Marcio L. Rodrigues,[2,9] Guilhem Janbon[1]

AUTHOR AFFILIATIONS See affiliation list on p. 18.

ABSTRACT Resistance to fluconazole (FLC), the most widely used antifungal drug, is typically achieved by altering the azole drug target and/or drug efflux pumps. Recent reports have suggested a link between vesicular trafficking and antifungal resistance. Here, we identified novel *Cryptococcus neoformans* regulators of extracellular vesicle (EV) biogenesis that impact FLC resistance. In particular, the transcription factor Hap2 does not affect the expression of the drug target or efflux pumps, yet it impacts the cellular sterol profile. Subinhibitory FLC concentrations also downregulate EV production. Moreover, *in vitro* spontaneous FLC-resistant colonies showed altered EV production, and the acquisition of FLC resistance was associated with decreased EV production in clinical isolates. Finally, the reversion of FLC resistance was associated with increased EV production. These data suggest a model in which fungal cells can regulate EV production in place of regulating the drug target gene expression as a first line of defense against antifungal assault in this fungal pathogen.

IMPORTANCE Extracellular vesicles (EVs) are membrane-enveloped particles that are released by cells into the extracellular space. Fungal EVs can mediate community interactions and biofilm formation, but their functions remain poorly understood. Here, we report the identification of the first regulators of EV production in the major fungal pathogen *Cryptococcus neoformans*. Surprisingly, we uncover a novel role of EVs in modulating antifungal drug resistance. Disruption of EV production was associated with altered lipid composition and changes in fluconazole susceptibility. Spontaneous azole-resistant mutants were deficient in EV production, while loss of resistance restored initial EV production levels. These findings were recapitulated in *C. neoformans* clinical isolates, indicating that azole resistance and EV production are coregulated in diverse strains. Our study reveals a new mechanism of drug resistance in which cells adapt to azole stress by modulating EV production.

KEYWORDS *Cryptococcus neoformans*, extracellular vesicles, antimicrobial resistance, fluconazole, transcription factor

Fungal diseases have been consistently neglected despite their increasing impact on human health. These eukaryotic pathogens infect ~1.5 billion people worldwide and lead to ~1.5 million deaths annually (1, 2). Over 90% of reported fungal-associated deaths are caused by species from four genera *Aspergillus*, *Cryptococcus*, *Candida*, or *Pneumocystis* (3). The species *Cryptococcus neoformans*, *Candida albicans*, *Candida auris,* and *Aspergillus fumigatus* form the critical priority group within the fungal pathogens list published by the World Health Organization in 2022 (4, 5). Fungal infections are generally difficult to treat, and mortality rates remain high despite available antifungal treatments (6). The arsenal of antifungal molecules is based on four main classes: polyenes (e.g.,

Editor Yong-Sun Bahn, Yonsei University, Seoul, Republic of Korea

Address correspondence to Guilhem Janbon, janbon@pasteur.fr.

The authors declare no conflict of interest.

See the funding table on p. 19.

Received 5 April 2023
Accepted 17 April 2023
Published 13 June 2023

Juliana Rizzo, Adèle Trottier, Frédérique Moyrand, Jean-Yves Coppee, Corinne Maufrais, Ana Claudia G. Zimbres, Thi Tuong Vi Dang, Isabelle Mouyna, Leonardo Nimrichter, Marcio L. Rodrigues, and Guilhem Janbon are members of the data sharing transparency group on fungal extracellular vesicles.

amphotericin B), azoles (e.g., fluconazole [FLC]), echinocandins (e.g., caspofungin), and flucytosine (a pyrimidine analog) (7). Due to their bioavailability, low toxicity, and wide spectrum of action, azoles are the most widely used antifungals. Azoles are fungistatic drugs that inhibit the cytochrome P450-dependent enzyme 14-α demethylase encoded by *ERG11* in fungi, thus interrupting the synthesis of ergosterol (6). In azole-treated cells, an accumulation of toxic intermediate sterols is observed, increasing membrane permeability and inhibiting fungal growth (8). Prolonged use of FLC has the potential to select FLC-resistant strains (8). Azole resistance has been associated with mutations in the *ERG11* sequence, thus limiting azole binding (8), or in transcription factors (TFs), like *TAC1* or *UPC1,* regulating the expression of *ERG11* and/or drug efflux pumps (9, 10). Heteroresistance has also been described in *C. neoformans* and was associated with the unstable duplication of chromosome 1, resulting in the potential overexpression of *ERG11* and the efflux pump-encoding gene *AFR1* (11, 12).

Extracellular vesicles (EVs) are cell-derived membrane particles released to the extracellular space known to be produced in all domains of life. In fungi, they have been isolated from at least 15 different genera (13). *Cryptococcus* EVs display extensive diversity in size, shape, and structure (14), and most EVs appear decorated by fibrillary material composed of mannoproteins and are covered by capsule polysaccharide-like material (14). EVs contain lipids (including ergosterol), polysaccharides, small molecules, pigments, and RNAs, although our understanding of the exact composition and function of these cargo molecules remains limited (15).

The involvement of vesicular trafficking in fungal FLC resistance has been previously suggested (16–18). For instance, turbinmicin, a molecule with a broad spectrum antifungal activity, targets Sec14p in the post-Golgi vesicular trafficking pathway and synergizes with FLC against *C. albicans* biofilm formation (19). Sortin2 inhibition of vesicular transport potentiates azoles in *C. albicans* and *C. glabrata* (18). Studies in *C. neoformans* and *Saccharomyces cerevisiae* have implicated Golgi trafficking and vesicle formation as potential avenues of azole potentiation (17, 20, 21). Recent studies also suggested that EVs released by fungi could play a role in antifungal resistance (22–25). For instance, *C. albicans* EVs confer FLC resistance to biofilms, and endosomal sorting complexes required for transport mutants defective in EVs production show altered biofilm FLC resistance (22). EVs from *C. auris* drug-resistant strain induced amphotericin-B resistance to a susceptible strain (23), but the mechanisms underlying this process remain largely unknown. Other examples of EVs associated with drug resistance come from the study of *Leishmania* parasites (26), where EVs mediate the delivery of drug-resistance genes, leading to the emergence of resistant subpopulations (26).

Despite these intriguing connections, the study of fungal EV biosynthesis in the context of antifungal resistance has been constrained by our limited understanding of EV biosynthesis. Genetic analyses of EV production and regulation have been hampered by the long and cumbersome protocols necessary to isolate and study these particles. Only a handful of mutations associated with defects in EV production have been reported so far, as recently reviewed (13).

To narrow this knowledge gap, we screened a *C. neoformans* TF mutant library (27) and identified the first regulators of EV biogenesis in fungi. We present data revealing a phenotypic association between drug resistance and regulation of EV biogenesis in these mutant strains but also in spontaneous FLC-resistant mutants isolated *in vitro,* as well as in clinical isolates. Moreover, we demonstrate that EV-defective mutants show altered lipid content. Finally, we show that subinhibitory concentrations of FLC regulate EV production. Taken together, our study points to a new mechanism of drug resistance in which cells adapt to FLC stress by modulating EV production. Our results uncover key regulators of EV biogenesis in *C. neoformans*, as well as a novel link with antifungal drug resistance.

RESULTS

EV production is regulated by growth conditions and growth phase in *C. neoformans*

To test whether EV production varies across different media, growth stages, and temperatures, we optimized a new EV isolation protocol, in which the ultracentrifugation step was bypassed (Fig. 1A). We used this protocol to demonstrate that EV production, as measured by the amount of total sterol in cellular supernatants, was highest when cells were grown in synthetic dextrose (SD) medium at 30°C compared with the other conditions tested (Fig. 1B). By exploring the dynamics of EV production during the growth on SD agar plates at 30°C, we noticed that cells release EVs during a limited time window (16–24 h) corresponding to the transition between the exponential and stationary growth phase (Fig. 1C).

Identification of regulators of EV production in *C. neoformans*

The tight regulation between EV production and growth suggested that specific TFs might regulate their biosynthesis. Thus, to identify potential regulators of EV biogenesis, we screened a collection of 155 TF mutants (27) using the EV purification optimized protocol adjusted to 96-well plates (Fig. 2A). We identified four mutants strongly altered in EV production. These strains produced < 10% of the wild-type (WT) EV levels as evaluated by the total amount of sterols in EV samples. The EV-deficient strains lacked TFs *BZP2* (CNAG_04263), *GAT5* (CNAG_05153), *LIV4* (CNAG_06283), and *HAP2* (CNAG_07435). These results were confirmed when samples were prepared using the conventional ultracentrifugation protocol (14), measuring the total amount of sterols (Fig. 2B), and evaluating the number of particles by nanoparticle flow cytometry (nanoFCM) analysis (Fig. 2C). It is important to note that despite an impressive decrease in EV levels, these TF mutants were not completely impaired in EV production, as the high sensitivity of the nanoFCM analysis used detected EV-like particles in each of the EV samples obtained from the mutants. Moreover, using a large number of culture plates, we obtained enough *hap2*Δ-derived EVs to be observed by Cryo-EM. Image analysis revealed a similar structure of *hap2*Δ EVs as previously observed for WT EVs (14) (Fig. 2D).

Bzp2p and Gat5p belong to a conserved zinc finger family containing TFs known as GATA-factors, regulating radiation sensitivity and nitrogen catabolite repression when

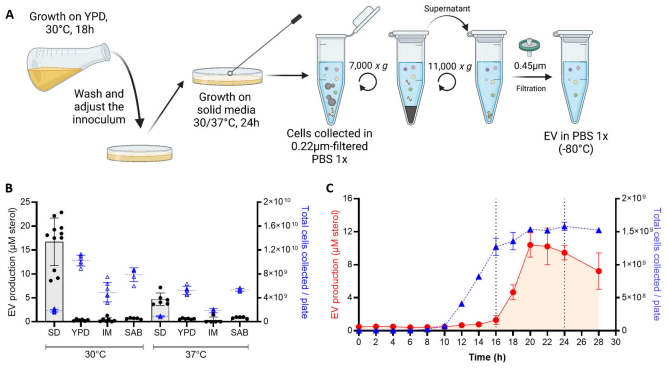

FIG 1 EV production is regulated by growth conditions and growth phase. Schematic representation of the optimized quick protocol used to obtain EVs from cells grown on solid medium (A). EV production from cells grown on different media: SD, YPD, capsule IM, and SAB at 30°C and 37°C, sterol concentration values are expressed per 10^9 cells for each condition (B). EV production on SD medium at 30°C during the growth curve was analyzed by the amount of total sterol in cellular supernatants when EVs are isolated using the quick protocol, values are expressed per plate of culture during each timepoint (C). Experiments were done with three or more biological replicates. Error bars show means ± SD. Schematic representation created in BioRender.

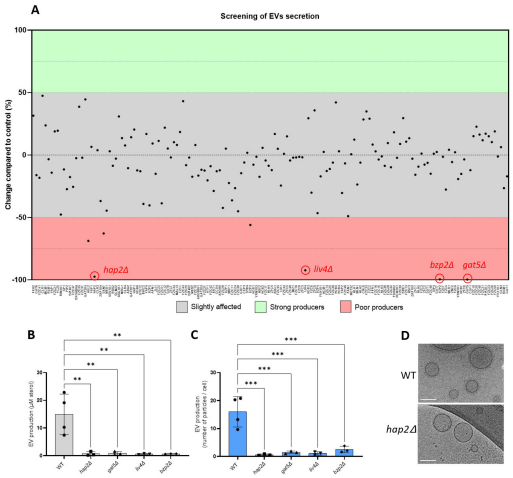

FIG 2 Identification of the transcription factors regulating EV production in *C. neoformans*. The screening of a 155 TF mutant collection identified four major EV production regulators: *HAP2*, *LIV4*, *BZP2*, and *GAT5* (A). Confirmation of the EV phenotype using independent knockout strains generated in the KN99α background by measuring the amount of total sterol contained in EV samples. Sterol concentration values are expressed per 10^9 cells for each condition (B) and single particle counting using nanoFCM (C). Cryo-electron microscopy (Cryo-EM) analysis of EVs obtained from WT and *hap2*Δ strains (D). Scale bars = 100 nm. Experiments were performed in at least three biological replicates. Error bars show means ± SD.

preferred nitrogen sources are absent or limiting (28). Liv4p is a conserved MYB-like DNA-binding domain TF, regulating growth and virulence in *C. neoformans* (29). Hap2p is a subunit of the evolutionary conserved CCAAT-binding heme activator protein (HAP) complex, a heterotrimeric complex composed of Hap2/3/5 and the transcriptional activation subunit, HapX (30). As expected, the *hap3*Δ and *hap5*Δ mutants were also drastically impaired for EV production. In contrast, the *hapX*Δ mutant strain produced the same quantity of EVs as the WT strain (Fig. 3A), suggesting that the Hap2/3/5 complex controls EV production in an HapX-independent manner in *C. neoformans*. Notably, whereas *bzp2*Δ, *liv4*Δ, and *gat5*Δ mutant strains displayed reduced growth (Fig. S1), none of the *hap* mutant strains showed growth deficiency under the conditions used to obtain EVs (Fig. 3D).

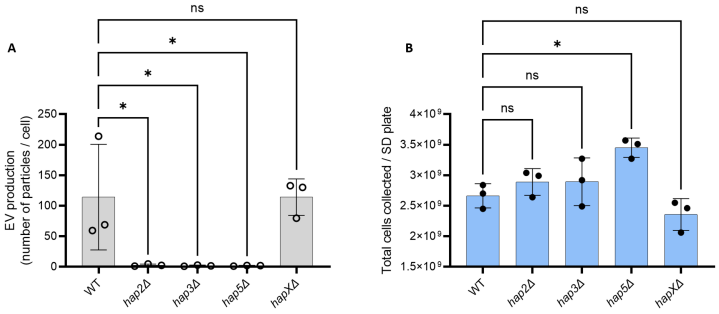

FIG 3 The *HAP2/3/5* complex is involved in EV secretion. Quantification of single EV particles released by WT and HAP complex mutants using nanoFCM (A). Growth analysis by counting the total number of cells obtained from SD plates (B). The experiments were carried out in biological triplicates. Error bars show means ± SD. ns, not significant;. *p < 0.05.

Transcriptional analysis of EV-defective mutants

To decipher the link between the expression of these TF and the EV production phenotype of their corresponding mutants, we performed the RNA-seq analysis of the *hap2*Δ, *gat5*Δ, and WT strains grown for 18 h on SD plates at 30°C, a condition which corresponds to the maximum EV production (see Fig. 1C). Differential expression gene analysis identified 538 genes commonly upregulated in both *hap2*Δ and *gat5*Δ strains (Fig. 4A) (Table S1). Gene ontology (GO) analysis using the FungiDB database (https://fungidb.org/fungidb/app) revealed that genes associated with ribosome biogenesis, transmembrane transport, and protein-containing complex assembly were enriched in this set (Fig. 4B). This suggests that the downregulation of the translation machinery expected to occur during the transition from the exponential phase to the stationary phase (31) is impaired in both mutant strains. On the other hand, 310 genes were downregulated in both mutant strains (Fig. 4C) (Table S1). GO analysis revealed genes coding for proteins implicated in protein glycosylation, signaling, carbohydrate metabolic processes, cell wall organization and biogenesis, protein modification process, carbohydrate metabolism, reproductive processes, vesicle-mediated transport, as well as cytokinesis, as being enriched in this set (Fig. 4D). Interestingly, *GAT5* expression is strongly downregulated (10-fold) in the *hap2*Δ mutant, suggesting that Hap2 might act upstream of Gat5 in regulating EV production. In contrast, neither *BZP2* nor *LIV4* appeared regulated by *HAP2* and/or *GAT5*, suggesting an independent regulation pathway. We then considered the top 100 most expressed genes in WT within the lists of *gat5*Δ, or *hap2*Δ downregulated genes reasoning that the impact of a gene downregulation associated with a mutation would have a phenotypic consequence if this gene is strongly expressed in the WT strain. Interestingly, 21 of the 39 previously identified *C. neoformans* enriched EV-associated protein-encoding genes (14) were regulated by either *GAT5* or *HAP2* (Fig. 4E). In addition, 15 genes coding for EV proteins regulated by both TFs included seven proteins belonging to the top 10 most abundant EV-associated proteins in *C. neoformans*. Thus, *HAP2* and *GAT5* regulate the expression of many EV-associated protein components, confirming their function as major regulators of EV production in *C. neoformans*.

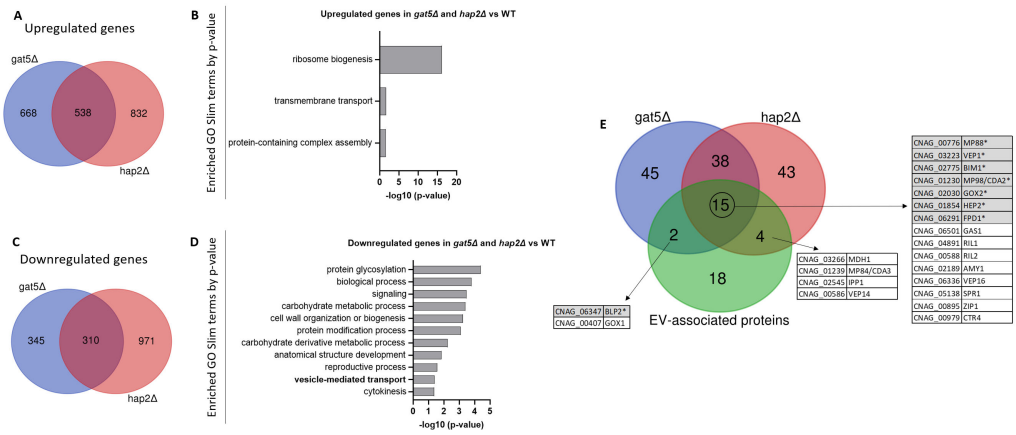

FIG 4 Transcriptomic analysis of the EV-deficient mutants *hap2*Δ and *gat5*Δ grown in EV-producing conditions. Venn diagram revealing the number of upregulated genes in both mutants (A). Analysis of the Go-slim categories enriched in the group of genes upregulated in both mutants (B). Venn diagram revealing the number of the downregulated genes in both mutants (C). GO SLIM categories enriched in the group of downregulated genes in both mutants (D). Venn diagram revealing the overlap between genes downregulated in *gat5*Δ and *hap2*Δ, and the ones coding for the EV-enriched proteins of *C. neoformans*, previously identified by proteomics (E). The genes highlighted in gray with an asterisk encode proteins among the 10 most abundant proteins in *C. neoformans* EVs.

EV production regulator mutant strains are altered in azole susceptibility

Strikingly, all four newly identified EV production mutant strains have been reported to have altered FLC sensitivity in the systematic phenotypic analysis of the TF mutants published by the Bahn's laboratory (27). Indeed, we confirmed that *hap2*Δ, *gat5*Δ, and *liv4*Δ were less susceptible to FLC, while *bzp2*Δ was more susceptible compared with the WT strain (Fig. 5A and B). Similar phenotypes were observed with itraconazole and voriconazole (Fig. 5A). We also tested the FLC susceptibility of the *hap* mutants and noticed that those impaired in EV production (i.e., *hap2Δ*, *hap3*Δ, and *hap5*Δ) were also more resistant to FLC. In contrast, the *hapX*Δ mutant strain, which showed no alteration in EV production (Fig. 3A), only displayed slight differences in FLC sensitivity (Fig. 5B).

Accordingly, reconstruction of the *gat5*Δ and *hap2*Δ mutant strains restored both phenotypes to WT levels (Fig. 6A through D). We also evaluated the sensitivity of these strains to agents that disturb the cell wall and plasma membrane, such as calcofluor white (CFW), hydrogen peroxide (H_2O_2), and sodium dodecyl sulfate (SDS), and observed that only *gat5Δ* was more susceptible to the presence of SDS (Fig. 6E). Overall the analysis of TF mutant strains suggested that EV production and FLC susceptibility are coregulated.

*hap2*Δ FLC resistance is not associated with *ERG11* or *AFR* genes over expression

In *C. neoformans,* FLC resistance has been associated with either mutation of *ERG11* (CNAG_00040) and/or the overexpression of efflux pumps genes such as *AFR1* (CNAG_00730), *AFR2* (CNAG_00869), and *AFR3* (CNAG_06909) (32). Interestingly, differential gene expression analysis of *gat5*Δ, *hap2*Δ, and WT cells grown under conditions of EV production revealed that neither mutation was associated with an increased expression of any of these resistance genes. We then used RT-qPCR assays to evaluate the expression levels of *ERG11* and the *AFR* genes in the presence or absence of FLC in these genetic backgrounds. As an additional control, we also included a strain lacking *NRG1* (CNAG_05222), which was shown to be FLC resistant (27) but was found here to produce WT EV levels (Fig. S2). In the absence of FLC, we did not observe changes in *ERG11* expression associated with either *HAP2* or *GAT5* deletion (Fig. 7A). In the presence of the drug, the expression of *ERG11* in the *hap2*Δ mutant strain was similar

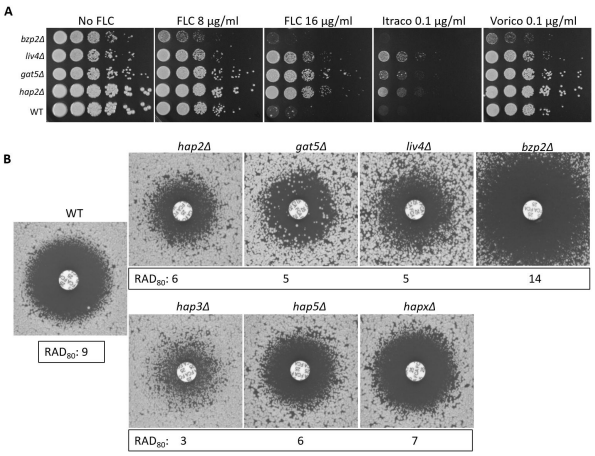

FIG 5 Transcription factors regulating EV release are associated with altered azole susceptibility. Spot assay for FLC, itraconazole (Itraco), and voriconazole (Vorico) susceptibility (A) and FLC diffusion disk diffusion assay (25 µg/disk) for the four EV-defective TF mutants identified in the screening (*hap2*Δ, *gat5*Δ, *liv4*Δ, and *bzp2*Δ), and for all the members of HAP complex, including *hap3*Δ, *hap5*Δ, and *hapX*Δ, grown for 72 h (B). Average RAD_{80} values obtained from diskImageR analyses are provided. The results are illustrative of three biological replicates.

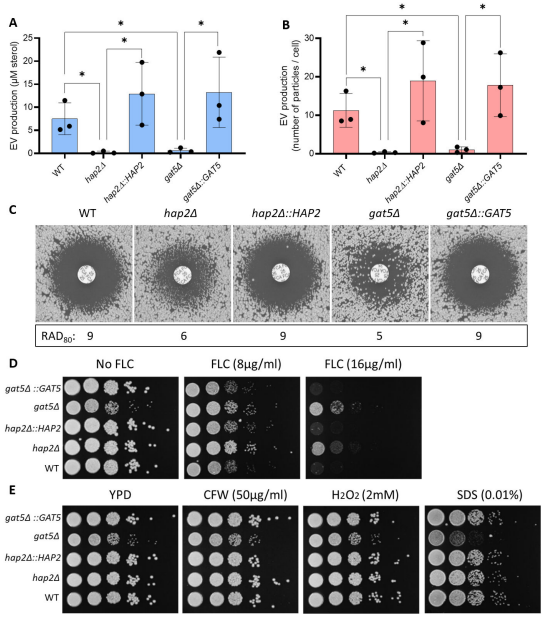

FIG 6 Complementation of the *hap2*Δ and *gat5*Δ mutant strains restores the phenotypes of EV production and FLC susceptibility. Total sterol contents in EVs produced by WT, mutants, and complemented cells. Sterol concentration values are expressed per 10^9 cells for each condition (A). Quantification of EV particles using nanoFCM in WT, mutants, and complemented strains (B). FLC susceptibility by disk diffusion assay (25 µg/disk) and RAD_{80} values obtained by diskImageR (C). FLC susceptibility analysis by spot assay (D). Growth analysis in the presence of cell wall and plasma membrane disturbing agents (CFW, H_2O_2, and SDS) (E). The experiments were carried out in biological triplicates. Error bars show means ± SD.

to the WT, whereas in *gat5*Δ, we observed a twofold reduction expression. In contrast, in the *nrg1*Δ mutant strain, we observed a twofold overexpression of *ERG11* as compared with the WT strain. Thus, the FLC resistance phenotype in *hap2*Δ and *gat5*Δ mutants cannot be explained by an alteration in *ERG11* expression levels (Fig. 7A).

In contrast to *ERG11*, the presence of FLC did not impact the expression of *AFR* genes in any of these strains (Fig. 7B through D). However, *AFR1* and *AFR3* but not *AFR2* were

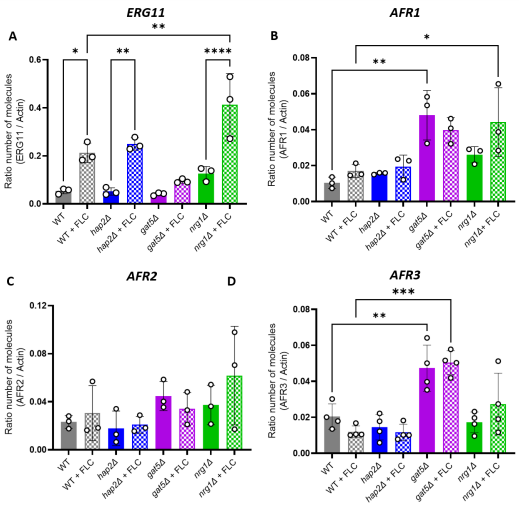

FIG 7 Gene expression analysis of known FLC resistance regulators in *C. neoformans*. *ERG11* (A), *AFR1* (B), *AFR2* (C), and *AFR3* (D) gene expression profile as generated by RT-qPCR. The experiments were carried out in at least biological triplicates. Error bars show means ± SD.

upregulated in the *gat5*Δ mutant (both with and without FLC), suggesting that these two efflux pumps could play a role in driving FLC resistance in this strain (Fig. 7B through D). A similar result was obtained with the *nrg1*Δ mutant, although to a lesser extent for *AFR3*. Interestingly, in the *hap2*Δ strain, the expression of the *AFR* genes was not altered, suggesting that additional mechanisms are driving FLC resistance in these cells.

FLC regulates EV production and cellular lipid profile

The analysis of the EV regulators suggests that changes in EV production impact FLC resistance. We then studied the converse relationship and tested whether FLC could modulate EV production in *C. neoformans*. We first tested the growth of WT cells on SD containing FLC at different concentrations (0.3, 0.6, 1.25, 2.5, and 5 µg/mL) identifying 0.6 µg/mL as the highest FLC concentration, which was not affecting cellular growth (Fig. 8A). At this concentration, the expression of *ERG11* was not altered (Fig. 8B). However, EV production was reduced by 2.4-fold (Fig. 8C), suggesting that FLC regulates EV production levels.

FLC is an inhibitor of the Erg11 lanosterol 14-α demethylase, which transforms lanosterol in 4,4-dimethyl-cholesta-8,14,24-trienol in the fungal ergosterol biosynthetic pathway (33). We thus compared the cellular lipid profile in WT and EV-defective mutant cells in the presence or absence of the same FLC-subinhibitory concentration (0.6 µg/mL). As expected (34), FLC treatment led to lanosterol accumulation in all strains under the growth conditions examined (Fig. 8D). However, decreased accumulation was observed in the *gat5*Δ and *hap2*Δ mutant strains as revealed by the ratio of lanosterol/ergosterol signals, suggesting that the lipid composition is altered in these EV-defective strains (Fig. 8E).

FLC-resistant isolates obtained *in vitro* are impaired in EV production

To further explore the link between FLC resistance and EV production in *C. neoformans*, we analyzed the EV production in spontaneous FLC-resistant isolates obtained *in vitro*. Previous studies reported that when *C. neoformans* cells are spread on a medium containing an inhibitory FLC concentration, a subset of the cell population can grow and produce colonies. This phenomenon is known as heteroresistance and was associated

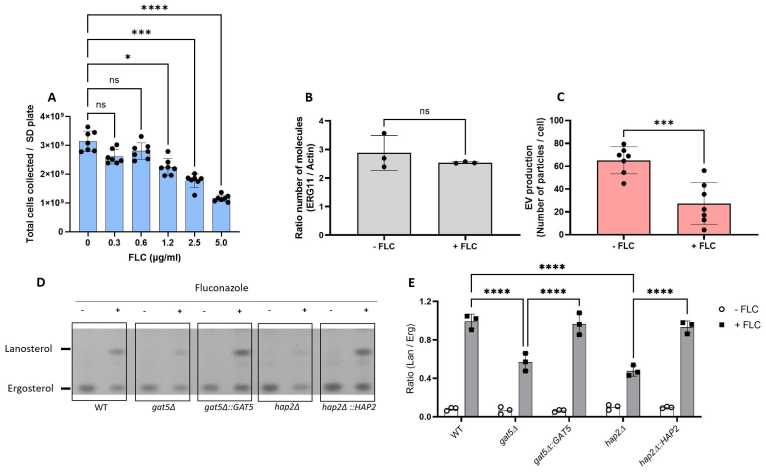

FIG 8 Fluconazole treatment affects EV production and cellular sterol homeostasis. WT cells were grown in different concentrations of FLC on SD agar medium, and the total number of cells was counted (A). Levels of *ERG11* expression in the presence of a subinhibitory concentration of FLC (0.6 µg/mL) (B). Analysis of EV production by nanoFCM in the presence of FLC (0.6 µg/mL) (C). Analysis of lanosterol and ergosterol lipid profile by TLC in cells (D). Analysis of TLC bands by densitometry units and ratio between lanosterol- and ergosterol-specific signals for cells (E). The experiments were carried out in at least two biological duplicates, and representative results were shown. Error bars show means ± SD. ns, not significant. *p < 0.05.

with the duplication of chromosome 1 bearing *ERG11* and *AFR1* resistance genes (12, 33, 35). This FLC-resistant phenotype can be reverted by subculturing the cells in a drug-free medium, the phenotypic reversion being associated with the reversion of the aneuploid genotype (11). Therefore, we isolated independent spontaneous FLC-resistant colonies on plates containing 15 µg/mL of FLC. FLC-susceptible parental and FLC-resistant isolates were then passaged six times in a liquid drug-free YPD. A schematic overview of the experimental design is delineated in Fig. 9A. All parental, resistant, and passage strains were tested for EV production and FLC sensitivity. As expected, 16 passage 0 (P0) strains isolated on plates containing FLC were resistant to FLC, as revealed by a significant decrease in the inhibition halo in FLC-disk diffusion assays (Fig. 9B and D). Interestingly, this drug-resistant phenotype was accompanied by a substantial reduction in EV production as analyzed by nanoFCM (Fig. 9C). Importantly, none of the 16 FLC-resistant isolates had pronounced growth defects in the SD medium, presenting the same transition time frame from the exponential to stationary phase (Fig. S3). In contrast, the passage 6 (P6) strains all lost their resistant phenotype, although to a different extent (Fig. 9E and G), and they also restored EV production to parental levels (Fig. 9F).

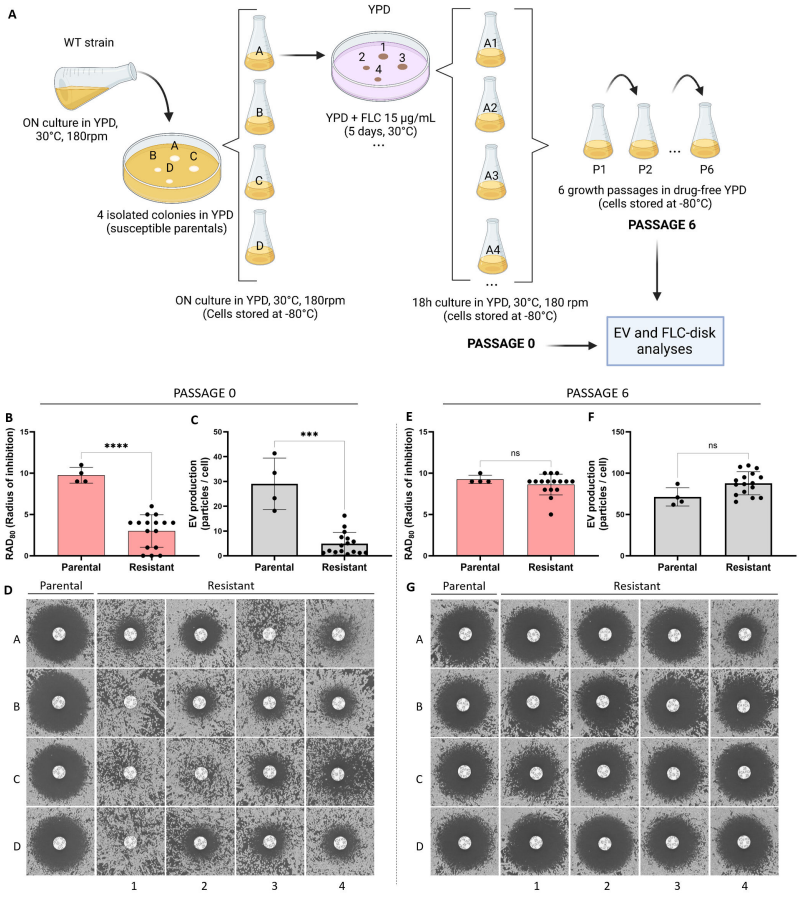

FIG 9 Analysis of FLC susceptibility and EV production in FLC-resistant isolates obtained *in vitro*. Illustrative scheme of the experimental strategy used to explore the association between FLC resistance and EV production in spontaneous drug-resistant strains obtained *in vitro* (A). Cells at passage 0: quantitative analysis of the growth inhibition halo from the FLC-disk diffusion assays by diskImageR, RAD_{80}(B), EV production analysis by nanoFCM (C), and qualitative analysis of the inhibition halo of the FLC-disk diffusion assays (D). Cells after six successive passages in the absence of FLC: quantitative analysis of growth inhibition halo from the FLC-disk diffusion assays by diskImageR, RAD_{80} (E), EV production analysis by nanoFCM (F), and qualitative analysis of the growth inhibition halo (G). Schematic representation created in BioRender.

We then evaluated the chromosome copy numbers of the parentals, FLC-resistant, and passaged strains by qPCR [using primers for genes located on chromosome 1 left arm (CNAG_00047), chromosome 1 right arm (CNAG_00483), and chromosome 2 (CNAG_03602)]. As expected, all parentals were monosomic for chromosome 1 (Fig. 10A and D). In agreement with the published literature, we also found that 14 out of 16 FLC-resistant strains were disomic for chromosome 1 (Fig. 10B and E). Meanwhile, all P6 strains reverted to the original monosomic state of chromosome 1 (Fig. 10C and F).

We sequenced the genomes of the A series to examine possible copy number variations. This analysis confirmed that strains A1 and A3 were disomic for chromosome 1, while strains A2 and A3 were disomic for chromosome 4 (Fig. 11A). Interestingly, while *ERG11* but not *AFR1* was overexpressed in the P0_A2 isolate, we found no change in the expression of these resistance genes in the P0_A4 isolate, suggesting that its FLC-resistant phenotype was independent of their regulation (Fig. 11B and C).

FLC resistance and regulation of EV release in *C. neoformans* clinical isolates

To test whether the relationship between EV production and FLC resistance would extend to clinical isolates, we studied a series of isolates having different levels of FLC susceptibility. Plotting the radius of inhibition (RAD_{80}) from FLC-disk diffusion assays and the average levels of EV production from these isolates did not reveal a clear correlation ($R^2 = 0.002$), as both the fully resistant isolates (no inhibition halo), as well as the most sensitive ones, were poor EV producers (Fig. 12A). We then considered serial isolates of *C. neoformans* that had become resistant during infection. For the isolates CNRMA17.247 and CNRMA20.738, we observed that the acquisition of FLC resistance coincided with the decreased ability to produce EVs (Fig. 12B). For the second lineage (isolates CNRMA4.1291 and CNRMA4.1293), we did not observe any difference in EV production between the sensitive and the resistant isolates (Fig. 12C). Interestingly, SNPs analysis revealed a CNRMA4.1293 specific (A to T) nonsynonymous mutation in *ERG11*, responsible for a Y145F mutation and possibly associated with the acquired resistance (36). We then tried to revert the resistance phenotype of four FLC-resistant clinical isolates (CNRMA20.738, CNRMA4.1293, CNRMA4.158, and CNRMA5.114) by growing them in a drug-free YPD medium for eight subsequent passages (P8). CNRMA5.114 was the only isolate for which we obtained a more sensitive derivative (Fig. 12D). In agreement with our previous observation, the P8-sensitive passage produced more EVs than the original P0-resistant isolate (Fig. 12E). As expected, P8 strains with no change in drug susceptibility also did not display altered EV production (Fig. 12D and E). Sequencing the genomes of the two lineages of recurrent isolates as well as the

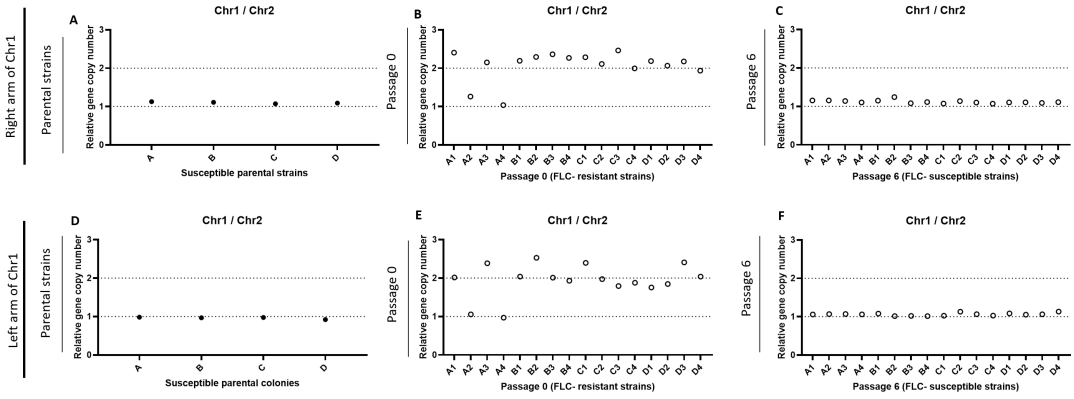

FIG 10 qPCR assays evaluating the monosomic or disomic status of chromosome 1 in the FLC-sensitive and FLC-resistant strains obtained *in vitro*. Parental strains (A, D), FLC-resistant passage 0 strains (B, E), and passage 6 strains (C, F) were tested using primers specific for genes located on chromosome 1 right (A–C) and left arms (D–F). Primers specific to chromosome 2 were used as control.

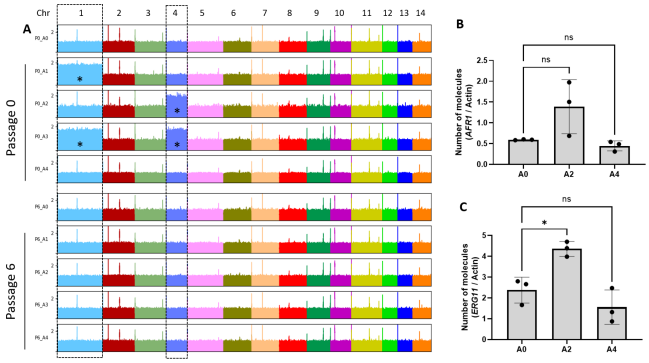

FIG 11 Chromosome duplications revealed after aligning DNA sequencing reads obtained from the A series of strains to the *C. neoformans* reference genome (A). *, chromosome duplication. Analysis of *AFR1* (B) and *ERG11* (C) gene expression in A0, A2, and A4 strains by RT-qPCR. ns, not significant. *p < 0.05.

P0 clinical isolates and their P8 derivatives revealed no chromosomal duplications (Fig. S4). Among the sequenced P0 clinical isolates, we observed the disomy of chromosome 12 in CNRMA5.114, which was lost in its P8-sensitive derivative. Partial duplication of chromosome 14 was also observed in the reverted P8 strain (Fig. 12F). We did not further investigate a possible causative link between FLC resistance and the observed genotype modifications in these isolates.

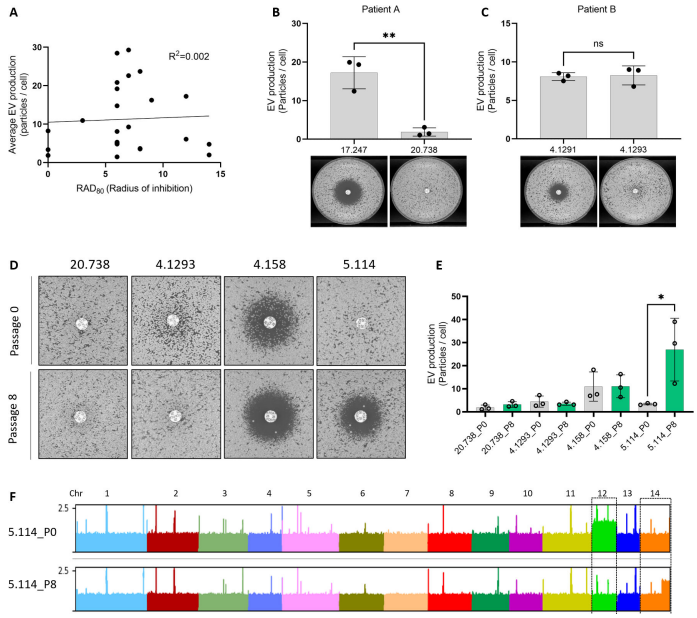

FIG 12 EV production and FLC resistance are linked in clinical isolates. Analysis of EV production by nanoFCM and size of FLC-disk inhibition halo in clinical isolates by linear regression (A, radius of inhibition=RAD_{80} values by diskImageR). EV production as measured by nanoFCM in the recurrent isolates CNRMA17.247 and CNRMA20.738 (top) and FLC-disk diffusion assays (bottom) from patient A (B). EV production as measured by nanoFCM in the recurrent isolates CNRMA4.1291 and CNRMA4.1293 (top) and FLC-disk diffusion assays (bottom) from patient B (C). FLC-disk diffusion assay in passaged clinical isolates. The CNRMA20.738 and CNRMA4.1293 passage 0 pictures are details of the ones presented in panels B and C, respectively (D). Analysis of EV production of passaged clinical isolates by nanoFCM (E). Alignment of DNA-Seq reads obtained from P0 and P8 CNRMA5.114 passaged clinical isolates (F). EV and FLC-disk analyses were carried out in at least biological triplicates, and representative results were shown. ns, not significant. *p < 0.05.

DISCUSSION

The mechanisms of biogenesis of EVs in fungi are still unknown. In this paper, we present experiments revealing a tight regulation of EV production in response to changes in growth conditions in *C. neoformans,* confirming previous reports in other models (37, 38). We also characterize four TF mutant strains strongly impaired in EV production, which are the first to be described in fungi and, to our knowledge, in any organisms. Surprisingly, we observed no major growth defect associated with *hap2*Δ mutation, suggesting that a WT level of EV production is dispensable in this fungus, at least under the examined conditions.

Our experiments also indicate that EV production is also strongly regulated by fungal growth phase. EVs are produced between 16 and 22 h after cell plating, corresponding to the transition between the exponential phase and the stationary phase. This result was consistent with reports of cells growing on YPD solid medium (38). In *S. cerevisiae*, the transition from the exponential phase to the stationary phase is associated with a shift from fermentation to respiration and a sharp slowdown of the general metabolism (39, 40). The Hap complex is the major regulator of this shift, controlling respiration and mitochondrial function in this yeast (41, 42). In pathogenic fungi, this complex has been studied mostly for its regulatory function in iron metabolism (43–45). As in *S. cerevisiae* (41), the Hap complex seems to control respiration in *C. neoformans*. Thus, Hap3 and HapX have also been shown to negatively regulate genes encoding respiratory and TCA cycle function under low iron condition (46). The *HAP* genes have also been shown to regulate sexual development in association with the pheromone-responsive Cpk1 mitogen-activated protein kinase pathway in this pathogenic yeast (42). However, phenotypic analyses of the *hap* mutants suggest that HapX and the Hap2/3/5 complex might also have independent functions. For instance, *HAP3* and *HAP5* but not *HAPX* are necessary for growth on ethanol (45), and the Hap2/3/5 complex, but not HapX, is crucial in repressing pheromone production and cell fusion during mating (42). Similarly, we found that the Hap2/3/5 complex, but not HapX, controls FLC resistance and EV production in *C. neoformans*.

The FLC resistance phenotype of the *hap* mutant strains is consistent with the literature (46, 47). Counterintuitively, Hap3 and HapX have been reported to positively regulate several ergosterol biosynthetic genes (46). Our differential gene expression analysis, which used different growth conditions, identified only two genes, *ERG20* (CNAG_02084) and *ERG27* (CNAG_07437) downregulated and one upregulated, *IDI1* (CNAG_00265) upon *HAP2* deletion. Overall, these data suggest that Hap2 in *C. neoformans* regulates global cellular changes impacting FLC resistance beyond the regulation of the ergosterol pathway.

In this work, we present cumulative lines of evidence suggesting a causative link between FLC resistance and EV production. First, all four EV production mutants displayed altered FLC susceptibility. We also observed this association with other hap mutants; *hapx*Δ being the only one producing WT level of EVs yet displaying a slight change in FLC susceptibilty. Second, all spontaneous FLC-resistant mutant strains isolated *in vitro* reduced the EV production, and both phenotypes reverted jointly. As many spontaneous FLC mutant strains are disomic for chromosome 1 (known to bear *ERG11* and *AFR1* [12]), one can imagine that repressors of EV production could also be located on this chromosome. Thus, chromosome 1 disomy could increase the expression of both FLC-resistant genes and EV repressors. However, we also identified two FLC-resistant spontaneous mutant strains with no duplication of chromosome 1; one being disomic of chromosome 4. Interestingly, none of the EV production regulators identified here are located on chromosome 1.

Finally, although we did not observe any correlations between the level of drug resistance and EV production among clinical isolates, the analysis of a couple of serial isolates from the same patient for which no mutation classically involved in FLC resistance could be identified revealed that the resistant strain produced lower EV amounts compared with the sensitive one. Notably, we did not observe any changes in

chromosome copy numbers in these strains. Moreover, a sensitive strain derived from a resistant clinical isolate obtained after several passages in a drug-free medium produces more EVs than the original strain. This reinforces the idea that EV production and FLC resistance are strongly linked, at least in a subset of genetic backgrounds.

Nevertheless, the molecular mechanism by which Hap2 and Gat5 regulate both EV production and FLC susceptibility remains unknown. Overexpression of the drug efflux pumps *AFR1* and *AFR3* in *gat5*Δ could contribute to the resistance phenotype. Similarly, disruption of the lanosterol/ergosterol equilibrium in the presence of FLC in the EV-deficient mutants could also impact drug resistance. Indeed, a recent report revealed that chemical disruption of the plasma homeostasis is sufficient to modify azole resistance in pathogenic fungi (48). However, it is unclear whether the decreased EV production alters plasma membrane homeostasis or whether these two TFs regulate membrane homeostasis and, consequently, EV production. Previous data in *Cryptococcus* suggest that the deletion of genes implicated in plasma membrane homeostasis can impact EV production and/or cargo loading (38, 49). On the other hand, the fact that most EV structural protein-encoding genes are strongly downregulated in both *gat5*Δ and *hap2*Δ mutants suggests a direct effect of these TF on EV biosynthesis. The fact that a Y145F *ERG11* mutation regulates FLC resistance without altering EV production also favors this second hypothesis.

Interestingly, we found that a low concentration of FLC reduces EV production. Yet, this concentration was not sufficient to alter the *ERG11* gene expression, suggesting that cells might regulate EV production to maintain plasma membrane homeostasis. The impact of low antifungal concentrations on fungal cell biology is poorly studied (6, 50), but our data clearly indicate that fungal cells might regulate EV production as a first line of defense under membrane stress. In this model (Fig. 13), FLC exposure triggers distinct types of cellular responses; *ERG11* overexpression and EV production would act to regulate plasma membrane homeostasis, whereas regulation of efflux pumps would minimize FLC concentrations in the cell.

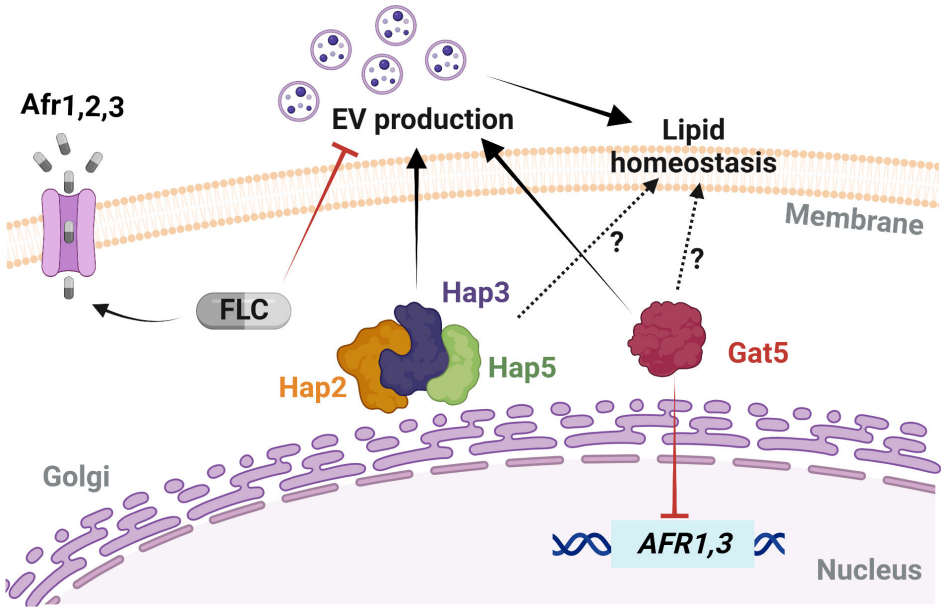

FIG 13 Model of EV biogenesis regulation and FLC susceptibility in *C. neoformans*. Specific gene mutations and FLC exposure can trigger diverse cellular responses, including changes in the expressions of drug efflux-associated genes, of the azole target gene, and in EVs biogenesis. Gat5 inhibits the expression of *AFR1* and *AFR3*, which can affect the intracellular FLC levels, while subinhibitory concentration of FLC can inhibit EV production. Hap2/3/5 and Gat5 regulate EV production, and cellular lipid homeostasis. The differential regulation of these cellular processes may determine FLC resistance phenotypes in this fungal pathogen. Schematic model created in BioRender.

Overall, this study identified the first TF regulating fungal EV biosynthetic pathways, while also uncovering novel roles that EVs play in modulating azole susceptibility. The genetics of EV production is still in its infancy, but functional genetics will further our understanding of EV biogenesis, their impact on drug resistance, and their roles during fungal infection.

MATERIALS AND METHODS

Media and culture conditions

All strains were taken from the G. Janbon laboratory collection at −80°C, plated onto yeast peptone dextrose (YPD) agar plates (1% yeast extract, 2% bacto-peptone, 2% dextrose, and 2% bacto-agar) and incubated at 30°C for 48 h before each experiment. Cell inoculum was performed in broth YPD (1% yeast extract, 2% bacto-peptone, and 2% dextrose) rotating at 180 rpm for 24 h at 30°C. The other solid media used in this study included Sabouraud (SAB) containing 1% bacto-peptone, 4% dextrose, 2% bacto-agar, SD containing 0.67% yeast nitrogen base (Difco) without amino acids, 2% glucose and 2% bacto-agar; and Capsule induction medium (IM) containing 1.7 g of yeast nitrogen base without amino acids and without ammonium sulfate (Difco), 1.5 g of asparagine and 20 g of glucose L^{-1} of buffer (12 mM in $NaHCO_3$, 35 mM in MOPS, pH 7.1), as previously described (51). Drug-containing plates were made by adding a stock solution of 3 mg/mL FLC powder in water to different final concentrations, depending on each experiment. The drug was added to the agar after autoclaving, then cooled to approximately 50°C before pouring.

Fungal strains and mutant construction

The *C. neoformans* TF mutant library (27) was obtained from the Fungal Genetic Stock Center (USA). This collection has been constructed in an H99o background (52). After the screening, the phenotype of the identified EV mutant strains was thus confirmed in the KN99α (53) background. All the following experiments have been performed in KN99α reference background. The strains used are listed in Table S2. The strains *MAT*α *hap2*Δ::*NAT* (CNAG_07435), *MAT*α *hap3*Δ::*NAT* (CNAG_02215), *MAT*α *hap5*Δ::*NAT* (CNAG_07680), *MAT*α *hapX*Δ::*NAT* (CNAG_01242), *MAT*α *gat5*Δ::*NAT* (CNAG_05153), and *MAT*α *nrg1*Δ::*NAT* (CNAG_05222) have been constructed in the Hiten Madhani lab (UCSF, USA) and obtained from the Fungal Genetic Stock Center. The genotypes of these mutant strains were confirmed by PCR using gene-specific internal primers. To construct the strains NE1539 (*MAT*α *bzp2*Δ::*NAT*) and NE1540 (*MAT*α *liv4*Δ::*NAT*), we replaced the entire CNAG_04263 (*BZP2*) and CNAG_06283 (*LIV4*) CDS by the NAT marker. The deletion cassettes construction and transformant screening were performed as previously described (54). The *GAT5* and *HAP2* genes were re-introduced into the corresponding mutant strain using a transient CRISPR-Cas9 expression system (55). DNA fragments spanning a genomic region from 1 kb upstream to 1 kb downstream the CDS of the genes were PCR amplified and cloned into the pSDMA57 plasmid before being integrated at the genomic "safe haven" locus in *gat5*Δ and *hap2*Δ mutants, respectively (56). All plasmids and primer sequences used are provided in Tables S3 and S4, respectively. Twenty-four clinical isolates of *C. neoformans* were also used. All isolates were recovered from the national cryptococcosis surveillance program managed by the National Reference Center for Invasive Mycoses & Antifungals (Institut Pasteur) between 2004 and 2021. All the clinical isolates are provided in Table S2.

EV isolation protocol and optimization for EV screening in 96-well plates

EV isolation by the conventional ultracentrifugation method followed the steps of the previously described protocol (14). A 96-format protocol was also used to test a large number of samples concomitantly. For this, cells from the stock were stacked on YPD

agar plates for 48 h at 30°C, and one loop of cells was inoculated in 1 mL of YPD broth of each well of a 96-deep well plate and incubated for 18 h at 30°C under agitation. The plate was centrifuged, and cells were washed two times with sterile water, adjusted to OD_{600} = 0.4 using a Tecan microplate reader (Tecan Trading AG, Switzerland). Then, 300 µL of the cell suspension was spread onto SD agar plates. After incubation for 24 h at 30°C, cells were gently recovered from the agar plates with an inoculation loop and suspended in 1 mL of 0.22-µm-filtered phosphate-buffered saline (PBS) 1 × in 2 mL Eppendorf tubes by pipetting up and down. The total number of cells collected from plates was evaluated by Coulter Counter (Z series, Beckman). Cells were centrifuged for 5 min at 7,000 × *g*; the supernatant was collected in a 1.5-mL tube and centrifuged again at 11,000 × *g* for 5 min. Supernatants were transferred to 96-well filter plates with 0.45-µm pore size and centrifuged at 2,500 × *g* for 3 min at 4°C. The filtered supernatants were kept at −80°C for further evaluations, including the quantification of EV single particles and EV size diameter by the Flow Nanoanalyser (57) (nanoFCM) and/or by measuring the total sterol amount by Amplex Red Cholesterol Assay Kit (Thermo Fisher Scientific, A12216), following the manufacturer's instructions.

In the TF mutant collection (27), each mutant is present as two or three independently obtained strains. Here, we first tested one mutant per gene. We then selected the most promising candidates producing less than 0.5-fold or more than 1.5-fold EVs compared with the WT strain. We then tested the second and third independent mutants when available in the collection. For all the mutants tested, the EV production was measured by the total amount of sterol normalized by the total number of cells collected for each strain. For the mutant strain 3.C10 (*gat1Δ*), which did not grow on SD plates, the EV production ratio was calculated based on mutant and WT growth on YPD agar plates.

Quantification of EV particles by nanoFCM

A NanoAnalyzer (nanoFCM) instrument equipped with a 488-nm laser at 50 mW and single-photon counting avalanche photodiodes detectors (SPCM APDs) was used for the detection of the EV particles. Band-pass filters allowed for the collection of light in specific channels (488/10 nm). Light scattering and fluorescence of individual EVs were collected on single-photon counting avalanche photodiodes detectors on three channels: side scatter (SSC)—488/10 (trigger channel). Sample fluid was focused to approximately 1.4 µm using an HPLC-grade water filter and de-gas as the sheath fluid via gravity feed. Data were generated through the Nanoanalyser Professional Suite V 2.0 software, 0.02-µm-filtered PBS was used to define the event triggering threshold. Measurements were taken over 1-min periods at a sampling pressure of approximately 1.0 kPa, modulated, and maintained by an air-based pressure module. Samples were diluted in 0.02-µm-filtered PBS as required to allow 3,000–13,000 counts to be recorded during this time. During data acquisition, the sample stream is completely illuminated within the central region of the focused laser beam, resulting in approximately 100% detection efficiency, which leads to accurate particle concentration measurement via single-particle enumeration. Optical alignment was tested and calibrated using fluorescent 250-nm silica nanoparticles. Further calibration measurements were taken prior to analysis using 250-nm silica nanoparticles of known concentration (for EV concentration calculation). Isolated EV samples were sized according to standard operating procedures using the proprietary four-modal silica nanosphere cocktail generated by nanoFCM to allow for a standard curve to be generated based on the four sizes of the nanosphere populations of 68, 91, 113, and 155 nm in diameter. Silica provides a stable and monodisperse standard with a refractive index of approximately 1.43–1.46, which is close to the range of refractive indices reported in the literature for EVs (n = 1.37–1.42). Using such a calibration standard enabled accurate flow cytometry size measurements, as confirmed when comparing flow cytometry with cryo-TEM results. The laser was set to 10 mW and 10% SSC decay. Data reported in the figure were handled within the nanoFCM Professional Suite v2.0 software to analyze particles between 40 and 155 nm.

DNA and RNA purification and sequencing libraries preparation

C. neoformans KN99α, *hap2*Δ, and *gat5*Δ strains were grown in EV production condition on SD for 18 h at 30°C. Cells were collected from the agar plates and suspended in 10 mL 0.22-µm-filtered PBS 1×. RNA extracts were prepared as previously described (58). Each condition was used to prepare biological triplicate samples. RNA-seq analysis was performed as previously described (59). Briefly, strand-specific, paired-end cDNA libraries were prepared from 1.5 µg of total RNA by polyA selection using the TruSeq Stranded mRNA kit (Illumina) according to the manufacturer's instructions. cDNA fragments of ~400 bp were purified from each library and confirmed for quality by Bioanalyzer (Agilent Technologies). DNA-Seq libraries from 2.5 µg of genome DNA were prepared using the TruSeq DNA PCR-free kit (Illumina). Then, 100 bases were sequenced from both ends using an Illumina NextSeq500 instrument according to the manufacturer's instructions (Illumina).

Sequencing library trimming and mapping

The paired reads from the RNA-seq libraries were trimmed for low-quality reads, and Illumina TruSeq adapters were removed with Cutadapt v1.9.1 (https://doi.org/10.14806/ej.17.1.200) with the following parameters: --trim-qualities 30 –e (maximum error rate) 0.1 --times 3 --overlap 6 --minimum-length 30. The cleaning of rRNA sequences was performed with Bowtie2 v2.3.3 (60) with default parameters; unmapped paired reads were reported using option --un-conc to identify reads that did not align with rRNA sequences. The cleaned reads from RNA-seq paired-end libraries from *C. neoformans* to the H99 reference genome (NCBI Genome Assembly GCA_000149245.3) with Tophat2 v2.0.14 (61) and the following parameters: minimum intron length 30; minimum intron coverage 30; minimum intron segment 30; maximum intron length 4000; maximum multihits 1; and microexon search. Analysis of differential expression data was performed in DeSeq2 (62).

DNA read alignment, variant detection, and ploidy analysis were performed as previously described (63). Illumina reads were aligned to the *C. neoformans* H99 reference genome using Minimap2 aligner v.2.9 (64) with the "-ax sr" parameter. BAM files were sorted and indexed using SAMtools (65) version 1.9. Picard version 2.8.1 (http://broadinstitute.github.io/picard) tools were used to identify duplicate reads and assign correct read groups to BAM files. SAMtools version 1.9 and Picard version 2.8.1 were then used to filter, sort, and convert SAM files and assign read groups, and mark duplicate reads. Single-nucleotide polymorphisms (SNPs) and insertions/deletions (indels) were called using Genome Analysis Toolkit version 3.6 with ploidy = 1 according to the GATK Best Practices. HaploScore parameters used to filter SNPs and indels included VariantFiltration, QD < 2.0, LowQD, ReadPosRankSum <−8.0, LowRankSum, FS >60.0, HightFS, MQRankSum <−12.5, MQRankSum, MQ < 40.0, LowMQ, and HaplotypeScore >13.0. To examine variations in ploidy across the genome, the sequencing depth at all positions was computed using SAMtools (65), and then the average depth was computed for 1 kb windows across the genome. GO analyses were performed using the FungiDB database (https://fungidb.org/fungidb/app).

Obtention of FLC-resistant *in vitro* strains and passaged derivatives

To obtain FLC-resistant *C. neoformans* strains *in vitro*, WT KN99α cells, previously grown for 24 h at 30°C, were plated on drug-free YPD agar plates and incubated for 48 h at 30°C. Four isolated parental colonies were used to inoculate four YPD liquid cultures grown ON at 30°C. An aliquot of the cells was stored at −80°C, and 1 mL of the culture was washed once with sterile water and adjusted to 10^5 cells/mL. About 200 µL of the cell suspension was plated on new YPD plates supplemented with FLC at 15 µg/mL and incubated for 5 days at 30°C. Four independent FLC-resistant colonies for each initial parental culture were collected from the plates, totalizing 16 resistant isolates. Each of these 16 strains was cultured in liquid YPD drug-free medium ON before being stored at

–80°C (P0 isolates). For the culture passages, susceptible parental cells and FLC-resistant derived strains were thawed on YPD agar plates (30°C) for 48 h. One small loop of the cells was inoculated in 1 mL of YPD in 96 deep well plates that were incubated under rotation at 30°C. Every 48 h, 10 µL of the cell suspension was collected and inoculated in 990 µL of fresh YPD using a multichannel. The remaining cells from each passage were centrifuged at 4,000 × rpm for 5 min (4°C), the supernatant was discarded, and the cell pellet was suspended in 200 µL of glycerol (40%) for keeping at –80°C. Parental strains and 96-well plates containing cells from passages 1 to 6 were stored at –80°C and further used for EV isolation and FLC-disk assays.

Disk diffusion and spot assays

Disk diffusion assays were performed as previously described (12), with minor adjustments. Cells were grown for 24 h in YPD broth at 30°C under agitation, centrifuged, washed once in sterile PBS 1×, and diluted at 1×10^6 cells/mL. About 100 µL of the cell suspension was spread onto YPD agar plates. A single 25 µg FLC disk (Bio-Rad) was placed in the center of each plate. Plates were incubated at 30°C for 48 and 72 h and photographed individually using a PhenoBooth+ (Singer Instrument, USA) apparatus. Analysis of the disk diffusion assay was done by ImageJ or by using the diskImageR pipeline, as previously described (66). Radius of inhibition levels, referred to as RAD throughout the manuscript, represents parameters measured at 80% drug inhibition (RAD_{80}). Cells for spot assays were prepared following the same steps previously described. Cells were diluted to 1×10^7 cells/mL and spotted (3 µL) in 10-fold serial dilutions onto the YPD plates containing the different drugs and compounds. The susceptibility assays were repeated a minimum of two times.

RT-qPCR for *ERG11*, *AFR1-AFR3* expression, and chromosomal ploidy analysis

For the analysis of gene expression by qPCR, three independent samples were prepared for each strain (WT, *hap2*Δ, *gat5*Δ, and *nrg1*Δ). Cells were cultured in YPD for 18 h at 30°C, under agitation. Then , 6.4×10^8 cells were transferred to 100 mL of YPD and grown for 4 h, at 30°C, under agitation. After the 4-h incubation, FLC was added at a final concentration of 10 µg/mL. We skipped this step in the control. Cell cultures were incubated for two additional hours at 30°C under agitation. Cells were counted and washed once with sterile water, and pellets were kept at –80°C for further RNA extraction, as previously described (51). Purified RNA was treated with DNase I recombinant, RNase-free (Roche) to eliminate residual genomic DNA. Synthesis of cDNA was performed using the Thermo Scientific Maxima First Strand cDNA Synthesis Kit for RT-qPCR, following the manufacturer's instructions. The expression levels of *ERG11* and *AFR1-AFR3* genes were determined by qPCR using 5 µL of the appropriate dilutions of cDNA and 1 µL of each primer of interest (10 µM), listed in Table S4. The reactions were performed using the SsoAdvanced Universal SYBR Green Supermix in Hard Shell qPCR plate 96-well thin wall (Bio-Rad). Amplification reactions were performed using an RT-PCR Detection System thermal cycler (Bio-Rad). The Ct values obtained in triplicates were averaged, and the number of molecules was measured by standard curves and normalized to that of the housekeeping gene *ACT1* (CNAG_00483). All RT-qPCR data were from three biological replicates (three independent RNA preparations).

We used qPCR assays and primers specific to the genes CNAG_00483, CNAG_00047, and CNAG_03602 to evaluate the copy number of the chromosome 1 right harm, chromosome 1 left harm, and chromosome 2, respectively (Table S4).

Lipid analysis by thin layer chromatography

Cells collected after 24 h grown on SD agar plates with or without FLC (0.6 µg/mL) were suspended in a mixture of chloroform (C) and methanol (M), C/M [2:1 (vol/vol)] and incubated for 4 h at room temperature. The suspension was clarified by centrifugation, and the supernatants were stored. Cell pellets were again extracted with a mixture of

C and M (1:2 [vol/vol]) under the same conditions. Supernatants containing the lipid extracts were combined and dried using a rotavapor (Heidolph, Germany). The resulting cell lipid extracts were submitted to a partition system composed of C/M/0.75% KCl in water (8:4:3 [vol/vol/vol]) and vigorously mixed. The lower phase was dried under an N_2 stream, weighed, and suspended in C to reach a concentration of 10 mg/mL of total cellular lipid extracted. To analyze cellular lipids, 50 µg of total lipid was spotted into thin layer chromatography (TLC) plates (silica gel 60 F_{254}; Merck, Germany). A total of 3 µL of purified lanosterol and ergosterol (1 mg/mL) were spotted in TLC plates as running standards. The plates were developed in chambers presaturated for 10 min at room temperature using cyclohexane and ethyl acetate (3:2 [vol/vol]) as a solvent running system. Plates were sprayed with a solution of 50 mg ferric chloride ($FeCl_3$) in a mixture of 90 mL water, 5 mL acetic acid, and 5 mL sulfuric acid. After heating at 100°C for 3–5 min, the sterol spots were identified by the appearance of a red–violet color. TLC plates were imaged, and the bands were densitometrically analyzed using ImageJ (NIH, USA). Values were expressed as ratios between cellular lanosterol and ergosterol-specific levels.

Statistical analysis

All statistical analyses were performed using GraphPad Prism 9 software (GraphPad Software Inc.). Data sets were tested for normal distribution using Shapiro–Wilk or Kolmogorov–Smirnov normality tests. In the cases in which the data passed the normality test, they were further analyzed using the unpaired Student's *t* test or ordinary one-way analysis of variance. When at least one data set was non-normally distributed, we used the nonparametric Kolmogorov–Smirnov or Kruskal–Wallis test.

ACKNOWLEDGMENTS

J.R. was supported by the Pasteur-Roux-Cantarini fellowship of Institut Pasteur and by FAPERJ - Fundação de Amparo à Pesquisa do Estado do Rio de Janeiro (E-26/204.456/2021). This work was supported by a CAPES COFECUB Grant no. 39712ZK to G.J., M.L.R., and L.N. The work was supported by an ANR grant (Projet ResistEV AAPG2021 CE35) to G.J., I.V.E., and A.A., T.T.V.D. was supported by the Pasteur - Paris University (PPU) International PhD Program. I.V.E. is supported by a CIFAR Azrieli Global Scholar Award.

We would like to thank in particular Laëtitia Viengsavanh for the help with the initial steps of TF mutant collection screening, and some members of the French Cryptococcosis Study Group: Christine Bonnal (Hôpital Bichat-Claude Bernardn Paris), Marie-Elisabeth Bougnoux (Hôpital Necker-Enfants Malades, Paris), Nathalie Bourgeois (CHU Montpellier), Sophie Cassaing (CHU Toulouse), Lilia Hasseine (CHU Nice), and Stéphane Ranque (IHU Méditerranée Infection, Marseille).

J.R., A.T., and F.M. performed the transcription factor mutant library screening for EV production, drug susceptibility assays, isolation of in vitro clinical isolates, growth passages and RT-qPCR analyses. F.M. and I.M. helped with the mutant construction. J.-Y.C. and J.R. prepared the DNA and RNA sequencing libraries. C.M. performed the sequencing library trimming, mapping and bioinformatic analyses. P.-H.C. and S.N. helped with the nanoflow cytometry analyses. I.V.E. advised on drug susceptibility assays and experimental design. G.P.-A. performed cryo-electron microscopy analyses. L.N. and A.C.G.Z. performed the lipid analysis. T.T.V.D. and J.R. performed the gene complementations. A.A and M.D.-O. selected the clinical strains to be studied. J.R. and G.J. conceived and designed the project. G.J. and M.L.R. supervised the research. J.R. and G.J. wrote the manuscript. All authors commented on the final version. All authors have read and agreed to the published version of the manuscript.

AUTHOR AFFILIATIONS

[1]Institut Pasteur, Université Paris Cité, Unité Biologie des ARN des Pathogènes Fongiques, Paris, France

[2]Instituto de Microbiologia Paulo de Góes (IMPG), Universidade Federal do Rio de Janeiro, Rio de Janeiro, Brazil
[3]Institut Pasteur, Université Paris Cité, USR 3756 IP CNRS, HUB Bioinformatique et Biostatistique, Paris, France
[4]Institut Pasteur, Université Paris Cité, Centre National de Référence Mycoses Invasives et Antifongiques, Groupe de recherche Mycologie Translationnelle, Département de Mycologie, Paris, France
[5]Laboratoire de parasitologie-mycologie, AP-HP, Hôpital Saint-Louis, Paris, France
[6]Institut Pasteur, Université Paris Cité, Plateforme de Bio-Imagerie Ultrastructurale, Paris, France
[7]Institut Pasteur, Université Paris Cité, Cytometry and Biomarkers, Paris, France
[8]Institut Pasteur, Université Paris Cité, Fungal Heterogeneity Group, Paris, France
[9]Instituto Carlos Chagas, Fundação Oswaldo Cruz (FIOCRUZ), Curitiba, Brazil

PRESENT ADDRESS

Juliana Rizzo, Instituto de Biofísica Carlos Chagas Filho (IBCCF), Universidade Federal do Rio de Janeiro, Rio de Janeiro, Brazil

AUTHOR ORCIDs

Alexandre Alanio http://orcid.org/0000-0001-9726-3082
Iuliana V. Ene http://orcid.org/0000-0002-0390-7084
Guilhem Janbon http://orcid.org/0000-0002-4788-1154

FUNDING

Funder	Grant(s)	Author(s)
Institut Pasteur	Pasteur-Roux-Cantarini Fellowship	Juliana Rizzo
Fundação Carlos Chagas Filho de Amparo à Pesquisa do Estado do Rio de Janeiro (FAPERJ)	E-26/204.456/2021	Juliana Rizzo
Coordenação de Aperfeiçoamento de Pessoal de Nível Superior (CAPES)	39712ZK	Leonardo Nimrichter Marcio L. Rodrigues Guilhem Janbon
Agence Nationale de la Recherche (ANR)	ResistEV AAPG2021 CE35	Alexandre Alanio Iuliana V Ene Guilhem Janbon
Institut Pasteur	Pasteur - Paris University (PPU) International PhD Program	Thi Tuong Vi Dang
Canadian Institute for Advanced Research (ICRA)	CIFAR Azrieli Global Scholar Award	Iuliana V Ene

AUTHOR CONTRIBUTIONS

Juliana Rizzo, Conceptualization, Investigation, Methodology, Writing – original draft, Writing – review and editing | Adèle Trottier, Investigation | Frédérique Moyrand, Investigation | Jean-Yves Coppée, Investigation | Corinne Maufrais, Investigation | Ana Claudia G. Zimbres, Investigation | Thi Tuong Vi Dang, Investigation | Alexandre Alanio, Methodology | Marie Desnos-Ollivier, Investigation | Isabelle Mouyna, Investigation | Gérard Péhau-Arnaude, Investigation | Pierre-Henri Commere, Investigation | Sophie Novault, Investigation | Iuliana V. Ene, Methodology, Writing – review and editing | Leonardo Nimrichter, Methodology, Supervision | Marcio L. Rodrigues, Methodology,

Supervision, Writing – review and editing | Guilhem Janbon, Conceptualization, Funding acquisition, Supervision, Writing – original draft, Writing – review and editing

DIRECT CONTRIBUTION

This article is a direct contribution from Guilhem Janbon, a Fellow of the American Academy of Microbiology, who arranged for and secured reviews by David R. Andes, University of Wisconsin-Madison, and Aaron P. Mitchell, University of Georgia.

DATA AVAILABILITY STATEMENT

Raw data are available at Bioproject: PRJNA928602.

ADDITIONAL FILES

The following material is available online.

Supplemental Material

Table S1 (mBio00870-23-s0001.xlsx). Genes regulated by HAP2 or GAT5 deletion.
Table S2 (mBio00870-23-s0002.xlsx). Strains used in this study.
Table S3 (mBio00870-23-s0003.xlsx). Plasmids used in this study.
Table S4 (mBio00870-23-s0004.xlsx). Primers used in this study.
Fig. S1 to S4 (mBio00870-23-s0005.docx). Supplemental figures.

REFERENCES

1. Fisher MC, Gurr SJ, Cuomo CA, Blehert DS, Jin H, Stukenbrock EH, Stajich JE, Kahmann R, Boone C, Denning DW, Gow NAR, Klein BS, Kronstad JW, Sheppard DC, Taylor JW, Wright GD, Heitman J, Casadevall A, Cowen LE. 2020. Threats posed by the fungal kingdom to humans, wildlife, and agriculture. mBio 11:e00449-20. https://doi.org/10.1128/mBio.00449-20
2. Janbon G, Quintin J, Lanternier F, d'Enfert C. 2019. Studying fungal pathogens of humans and fungal infections: fungal diversity and diversity of approaches. Genes Immun 20:403–414. https://doi.org/10.1038/s41435-019-0071-2
3. Brown GD, Denning DW, Gow NAR, Levitz SM, Netea MG, White TC. 2012. Hidden killers: human fungal infections. Sci Transl Med 4:165rv13. https://doi.org/10.1126/scitranslmed.3004404
4. Anonymous. 2022. Who fungal priority pathogens list to guide research, development and public health action. Available from: https://www.who.int/publications-detail-redirect/9789240060241
5. Rajasingham R, Smith RM, Park BJ, Jarvis JN, Govender NP, Chiller TM, Denning DW, Loyse A, Boulware DR. 2017. Global burden of disease of HIV-associated cryptococcal meningitis: an updated analysis. Lancet Infect Dis 17:873–881. https://doi.org/10.1016/S1473-3099(17)30243-8
6. Fisher MC, Alastruey-Izquierdo A, Berman J, Bicanic T, Bignell EM, Bowyer P, Bromley M, Brüggemann R, Garber G, Cornely OA, Gurr SJ, Harrison TS, Kuijper E, Rhodes J, Sheppard DC, Warris A, White PL, Xu J, Zwaan B, Verweij PE. 2022. Tackling the emerging threat of antifungal resistance to human health. Nat Rev Microbiol 20:557–571. https://doi.org/10.1038/s41579-022-00720-1
7. Almeida F, Rodrigues ML, Coelho C. 2019. The still underestimated problem of fungal diseases worldwide. Front Microbiol 10:214. https://doi.org/10.3389/fmicb.2019.00214
8. Robbins N, Caplan T, Cowen LE. 2017. Molecular evolution of antifungal drug resistance. Annu Rev Microbiol 71:753–775. https://doi.org/10.1146/annurev-micro-030117-020345
9. Berman J, Krysan DJ. 2020. Drug resistance and tolerance in fungi. Nat Rev Microbiol 18:319–331. https://doi.org/10.1038/s41579-019-0322-2
10. Rodero L, Mellado E, Rodriguez AC, Salve A, Guelfand L, Cahn P, Cuenca-Estrella M, Davel G, Rodriguez-Tudela JL. 2003. G484S amino acid substitution in Lanosterol 14-A demethylase (Erg11) is related to fluconazole resistance in a recurrent *Cryptococcus neoformans* clinical isolate. Antimicrob Agents Chemother 47:3653–3656. https://doi.org/10.1128/AAC.47.11.3653-3656.2003
11. Sionov E, Lee H, Chang YC, Kwon-Chung KJ. 2010. *Cryptococcus neoformans* overcomes stress of azole drugs by formation of disomy in specific multiple chromosomes. PLoS Pathog 6:e1000848. https://doi.org/10.1371/journal.ppat.1000848
12. Stone NR, Rhodes J, Fisher MC, Mfinanga S, Kivuyo S, Rugemalila J, Segal ES, Needleman L, Molloy SF, Kwon-Chung J, Harrison TS, Hope W, Berman J, Bicanic T. 2019. Dynamic ploidy changes drive fluconazole resistance in human cryptococcal meningitis. J Clin Invest 129:999–1014. https://doi.org/10.1172/JCI124516
13. Rizzo J, Rodrigues ML, Janbon G. 2020. Extracellular vesicles in fungi: past, present, and future perspectives. Front Cell Infect Microbiol 10:346. https://doi.org/10.3389/fcimb.2020.00346
14. Rizzo J, Wong SSW, Gazi AD, Moyrand F, Chaze T, Commere P-H, Novault S, Matondo M, Péhau-Arnaudet G, Reis FCG, Vos M, Alves LR, May RC, Nimrichter L, Rodrigues ML, Aimanianda V, Janbon G. 2021. *Cryptococcus* extracellular vesicles properties and their use as vaccine platforms. J Extracell Vesicles 10:e12129. https://doi.org/10.1002/jev2.12129
15. Rizzo J, Taheraly A, Janbon G. 2021. Structure, composition and biological properties of fungal extracellular Vesicles. microLife 2:1–13. https://doi.org/10.1093/femsml/uqab009
16. Khandelwal NK, Wasi M, Nair R, Gupta M, Kumar M, Mondal AK, Gaur NA, Prasad R. 2019. Vacuolar sequestration of azoles, a novel strategy of azole antifungal resistance conserved across pathogenic and nonpathogenic yeast. Antimicrob Agents Chemother 63:e01347-18. https://doi.org/10.1128/AAC.01347-18
17. Walton FJ, Heitman J, Idnurm A. 2006. Conserved elements of the ram signaling pathway establish cell polarity in the basidiomycete *Cryptococcus neoformans* in a divergent fashion from other fungi. Mol Biol Cell 17:3768–3780. https://doi.org/10.1091/mbc.e06-02-0125
18. Demuyser L, Van Dyck K, Timmermans B, Van Dijck P. 2019. Inhibition of vesicular transport influences fungal susceptibility to fluconazole. Antimicrob Agents Chemother 63:e01998-18. https://doi.org/10.1128/AAC.01998-18
19. Zhao M, Zhang F, Zarnowski R, Barns K, Jones R, Fossen J, Sanchez H, Rajski SR, Audhya A, Bugni TS, Andes DR. 2021. Turbinmicin inhibits *Candida* biofilm growth by disrupting fungal vesicle-mediated trafficking. J Clin Invest 131:e145123. https://doi.org/10.1172/JCI145123

20. Estrada AF, Muruganandam G, Prescianotto-Baschong C, Spang A. 2015. The arfgap2/3 glo3 and ergosterol collaborate in transport of a subset of cargoes. Biol Open 4:792–802. https://doi.org/10.1242/bio.011528
21. Wambaugh MA, Denham ST, Ayala M, Brammer B, Stonhill MA, Brown JC. 2020. Synergistic and antagonistic drug interactions in the treatment of systemic fungal infections. Elife 9:e54160. https://doi.org/10.7554/eLife.54160
22. Zarnowski R, Sanchez H, Covelli AS, Dominguez E, Jaromin A, Bernhardt J, Mitchell KF, Heiss C, Azadi P, Mitchell A, Andes DR. 2018. Candida albicans biofilm-induced vesicles confer drug resistance through matrix biogenesis. PLoS Biol 16:e2006872. https://doi.org/10.1371/journal.pbio.2006872
23. Chan W, Chow FW-N, Tsang C-C, Liu X, Yao W, Chan TT-Y, Siu GK-H, Ho AY-M, Luk KS, Lau SK-P, Woo PC-Y. 2022. Induction of amphotericin B resistance in susceptible *Candida auris* by extracellular vesicles. Emerg Microbes Infect 11:1900–1909. https://doi.org/10.1080/22221751.2022.2098058
24. Zarnowski R, Noll A, Chevrette MG, Sanchez H, Jones R, Anhalt H, Fossen J, Jaromin A, Currie C, Nett JE, Mitchell A, Andes DR. 2021. Coordination of fungal biofilm development by extracellular vesicle cargo. Nat Commun 12:6235. https://doi.org/10.1038/s41467-021-26525-z
25. Zhao K, Bleackley M, Chisanga D, Gangoda L, Fonseka P, Liem M, Kalra H, Al Saffar H, Keerthikumar S, Ang C-S, Adda CG, Jiang L, Yap K, Poon IK, Lock P, Bulone V, Anderson M, Mathivanan S. 2019. Extracellular vesicles secreted by *Saccharomyces cerevisiae* are involved in cell wall remodelling. Commun Biol 2:305. https://doi.org/10.1038/s42003-019-0538-8
26. Douanne N, Dong G, Amin A, Bernardo L, Blanchette M, Langlais D, Olivier M, Fernandez-Prada C. 2022. *Leishmania* parasites exchange drug-resistance genes through extracellular vesicles. Cell Rep 40:111121. https://doi.org/10.1016/j.celrep.2022.111121
27. Jung K-W, Yang D-H, Maeng S, Lee K-T, So Y-S, Hong J, Choi J, Byun H-J, Kim H, Bang S, Song M-H, Lee J-W, Kim MS, Kim S-Y, Ji J-H, Park G, Kwon H, Cha S, Meyers GL, Wang LL, Jang J, Janbon G, Adedoyin G, Kim T, Averette AK, Heitman J, Cheong E, Lee Y-H, Lee Y-W, Bahn Y-S. 2015. Systematic functional profiling of transcription factor networks in *Cryptococcus neoformans*. Nat Commun 6:6757. https://doi.org/10.1038/ncomms7757
28. Cui W, Li X, Hull L, Xiao M. 2019. Gata-Type transcription factors play a vital role in radiation sensitivity of *Cryptococcus neoformans* by regulating the gene expression of specific amino acid permeases. Sci Rep 9:6385. https://doi.org/10.1038/s41598-019-42778-7
29. Yi J, Sang J, Zhao J, Gao L, Yang Y, Yan L, Zhang C, Pan W, Wang G, Liao W. 2020. Transcription factor liv4 is required for growth and pathogenesis of *Cryptococcus neoformans*. FEMS Yeast Res 20:foaa015. https://doi.org/10.1093/femsyr/foaa015
30. Mao Y, Chen C. 2019. The Hap complex in yeasts: structure, assembly mode, and gene regulation. Front Microbiol 10:1645. https://doi.org/10.3389/fmicb.2019.01645
31. Fuge EK, Braun EL, Werner-Washburne M. 1994. Protein synthesis in long-term stationary-phase cultures of *Saccharomyces cerevisiae*. J Bacteriol 176:5802–5813. https://doi.org/10.1128/jb.176.18.5802-5813.1994
32. Gow NAR, Johnson C, Berman J, Coste AT, Cuomo CA, Perlin DS, Bicanic T, Harrison TS, Wiederhold N, Bromley M, Chiller T, Edgar K. 2022. The importance of antimicrobial resistance in medical mycology. Nat Commun 13:5352. https://doi.org/10.1038/s41467-022-32249-5
33. Jordá T, Puig S. 2020. Regulation of ergosterol biosynthesis in *Saccharomyces cerevisiae*. Genes (Basel) 11:795. https://doi.org/10.3390/genes11070795
34. Foresti O, Ruggiano A, Hannibal-Bach HK, Ejsing CS, Carvalho P. 2013. Sterol homeostasis requires regulated degradation of squalene monooxygenase by the ubiquitin ligase Doa10/Teb4. Elife 2:e00953. https://doi.org/10.7554/eLife.00953
35. Mondon P, Petter R, Amalfitano G, Luzzati R, Concia E, Polacheck I, Kwon-Chung KJ. 1999. Heteroresistance to fluconazole and voriconazole in *Cryptococcus neoformans*. Antimicrob Agents Chemother 43:1856–1861. https://doi.org/10.1128/AAC.43.8.1856
36. Sionov E, Chang YC, Garraffo HM, Dolan MA, Ghannoum MA, Kwon-Chung KJ. 2012. Identification of a *Cryptococcus neoformans* cytochrome P450 lanosterol 14α-demethylase (ERG11) residue critical for differential susceptibility between fluconazole/voriconazole and itraconazole/posaconazole. Antimicrob Agents Chemother 56:1162–1169. https://doi.org/10.1128/AAC.05502-11
37. Cleare LG, Zamith D, Heyman HM, Couvillion SP, Nimrichter L, Rodrigues ML, Nakayasu ES, Nosanchuk JD. 2020. Media matters! alterations in the loading and release of *Histoplasma capsulatum* extracellular vesicles in response to different nutritional milieus. Cell Microbiol 22:e13217. https://doi.org/10.1111/cmi.13217
38. Reis FCG, Borges BS, Jozefowicz LJ, Sena BAG, Garcia AWA, Medeiros LC, Martins ST, Honorato L, Schrank A, Vainstein MH, Kmetzsch L, Nimrichter L, Alves LR, Staats CC, Rodrigues ML. 2019. A novel protocol for the isolation of fungal extracellular vesicles reveals the participation of a putative scramblase in polysaccharide export and capsule construction in *Cryptococcus gattii*. mSphere 4:e00080-19. https://doi.org/10.1128/mSphere.00080-19
39. Werner-Washburne M, Braun E, Johnston GC, Singer RA. 1993. Stationary phase in the yeast *Saccharomyces cerevisiae*. Microbiol Rev 57:383–401. https://doi.org/10.1128/mr.57.2.383-401.1993
40. Galdieri L, Mehrotra S, Yu S, Vancura A. 2010. Transcriptional regulation in yeast during diauxic shift and stationary phase. OMICS 14:629–638. https://doi.org/10.1089/omi.2010.0069
41. Buschlen S, Amillet JM, Guiard B, Fournier A, Marcireau C, Bolotin-Fukuhara M. 2003. The *S. cerevisiae* Hap complex, a key regulator of mitochondrial function, coordinates nuclear and mitochondrial gene expression. Comp Funct Genomics 4:37–46. https://doi.org/10.1002/cfg.254
42. Bolotin-Fukuhara M. 2017. Thirty years of the HAP2/3/4/5 complex. Biochim Biophys Acta Gene Regul Mech 1860:543–559. https://doi.org/10.1016/j.bbagrm.2016.10.011
43. Singh RP, Prasad HK, Sinha I, Agarwal N, Natarajan K. 2011. Cap2-HAP complex is a critical transcriptional regulator that has dual but contrasting roles in regulation of iron homeostasis in *Candida albicans*. J Biol Chem 286:25154–25170. https://doi.org/10.1074/jbc.M111.233569
44. Gsaller F, Hortschansky P, Beattie SR, Klammer V, Tuppatsch K, Lechner BE, Rietzschel N, Werner ER, Vogan AA, Chung D, Mühlenhoff U, Kato M, Cramer RA, Brakhage AA, Haas H. 2014. The Janus transcription factor HapX controls fungal adaptation to both iron starvation and iron excess. EMBO J 33:2261–2276. https://doi.org/10.15252/embj.201489468
45. Jung WH, Saikia S, Hu G, Wang J, Fung CK-Y, D'Souza C, White R, Kronstad JW. 2010. Hapx positively and negatively regulates the transcriptional response to iron deprivation in *Cryptococcus neoformans*. PLoS Pathog 6:e1001209. https://doi.org/10.1371/journal.ppat.1001209
46. Kim J, Cho Y-J, Do E, Choi J, Hu G, Cadieux B, Chun J, Lee Y, Kronstad JW, Jung WH. 2012. A defect in iron uptake enhances the susceptibility of *Cryptococcus neoformans* to azole antifungal drugs. Fungal Genet Biol 49:955–966. https://doi.org/10.1016/j.fgb.2012.08.006
47. Caza M, Hu G, Price M, Perfect JR, Kronstad JW. 2016. The zinc finger protein Mig1 regulates mitochondrial function and azole drug susceptibility in the pathogenic fungus *Cryptococcus neoformans*. mSphere 1:e00080-15. https://doi.org/10.1128/mSphere.00080-15
48. Revie NM, Iyer KR, Maxson ME, Zhang J, Yan S, Fernandes CM, Meyer KJ, Chen X, Skulska I, Fogal M, Sanchez H, Hossain S, Li S, Yashiroda Y, Hirano H, Yoshida M, Osada H, Boone C, Shapiro RS, Andes DR, Wright GD, Nodwell JR, Del Poeta M, Burke MD, Whitesell L, Robbins N, Cowen LE. 2022. Targeting fungal membrane homeostasis with imidazopyrazoindoles impairs azole resistance and biofilm formation. Nat Commun 13:3634. https://doi.org/10.1038/s41467-022-31308-1
49. Rizzo J, Oliveira DL, Joffe LS, Hu G, Gazos-Lopes F, Fonseca FL, Almeida IC, Frases S, Kronstad JW, Rodrigues ML. 2014. Role of the APT1 protein in polysaccharide secretion by *Cryptococcus neoformans*. Eukaryot Cell 13:715–726. https://doi.org/10.1128/EC.00273-13
50. Handelman M, Osherov N. 2022. Experimental and in-host evolution of Triazole resistance in human pathogenic Fungi. Front Fungal Biol 3:1–21. https://doi.org/10.3389/ffunb.2022.957577
51. Janbon G, Himmelreich U, Moyrand F, Improvisi L, Dromer F. 2001. Cas1p is a membrane protein necessary for the *O*-acetylation of the *Cryptococcus neoformans* capsular polysaccharide. Mol Microbiol 42:453–467. https://doi.org/10.1046/j.1365-2958.2001.02651.x
52. Janbon G, Ormerod KL, Paulet D, Byrnes EJ, Yadav V, Chatterjee G, Mullapudi N, Hon C-C, Billmyre RB, Brunel F, Bahn Y-S, Chen W, Chen Y, Chow EWL, Coppée J-Y, Floyd-Averette A, Gaillardin C, Gerik KJ, Goldberg J, Gonzalez-Hilarion S, Gujja S, Hamlin JL, Hsueh Y-P, Ianiri G, Jones S,

Kodira CD, Kozubowski L, Lam W, Marra M, Mesner LD, Mieczkowski PA, Moyrand F, Nielsen K, Proux C, Rossignol T, Schein JE, Sun S, Wollschlaeger C, Wood IA, Zeng Q, Neuvéglise C, Newlon CS, Perfect JR, Lodge JK, Idnurm A, Stajich JE, Kronstad JW, Sanyal K, Heitman J, Fraser JA, Cuomo CA, Dietrich FS. 2014. Analysis of the genome and transcriptome of *Cryptococcus neoformans* var. *grubii* reveals complex RNA expression and Microevolution leading to virulence attenuation. PLoS Genet 10:e1004261. https://doi.org/10.1371/journal.pgen.1004261

53. Nielsen K, Cox GM, Wang P, Toffaletti DL, Perfect JR, Heitman J. 2003. Sexual cycle of *Cryptococcus neoformans* var. *grubii* and virulence of congenic a and alpha isolates. Infect Immun 71:4831–4841. https://doi.org/10.1128/IAI.71.9.4831-4841.2003
54. Moyrand F, Fontaine T, Janbon G. 2007. Systematic capsule gene disruption reveals the central role of galactose metabolism on *Cryptococcus neoformans* virulence. Mol Microbiol 64:771–781. https://doi.org/10.1111/j.1365-2958.2007.05695.x
55. lin J, Fan Y, Lin X. 2020. Transformation of *Cryptococcus neoformans* by electroporation using a transient CRISPR-Cas9 expression (TRACE) system. Fungal Genetics and Biology 138:103364. https://doi.org/10.1016/j.fgb.2020.103364
56. Arras SDM, Chitty JL, Blake KL, Schulz BL, Fraser JA. 2015. A genomic safe haven for mutant complementation in *Cryptococcus neoformans*. PLoS One 10:e0122916. https://doi.org/10.1371/journal.pone.0122916
57. Tian Y, Gong M, Hu Y, Liu H, Zhang W, Zhang M, Hu X, Aubert D, Zhu S, Wu L, Yan X. 2020. Quality and efficiency assessment of six extracellular vesicle isolation methods by nano-flow cytometry. J Extracell Vesicles 9:1697028. https://doi.org/10.1080/20013078.2019.1697028
58. Moyrand F, Lafontaine I, Fontaine T, Janbon G. 2008. *UGE1* and *UGE2* regulate the UDP-glucose/UDP-galactose equilibrium in *Cryptococcus neoformans*. Eukaryot Cell 7:2069–2077. https://doi.org/10.1128/EC.00189-08
59. Wallace EWJ, Maufrais C, Sales-Lee J, Tuck LR, de Oliveira L, Feuerbach F, Moyrand F, Natarajan P, Madhani HD, Janbon G. 2020. Quantitative global studies reveal differential translational control by start codon context across the fungal Kingdom. Nucleic Acids Res 48:2312–2331. https://doi.org/10.1093/nar/gkaa060
60. Langmead B, Trapnell C, Pop M, Salzberg SL. 2009. Ultrafast and memory-efficient alignment of short DNA sequences to the human genome. Genome Biol 10:R25. https://doi.org/10.1186/gb-2009-10-3-r25
61. Kim D, Pertea G, Trapnell C, Pimentel H, Kelley R, Salzberg SL. 2013. TopHat2: accurate alignment of transcriptomes in the presence of insertions, deletions and gene fusions. Genome Biol 14:R36. https://doi.org/10.1186/gb-2013-14-4-r36
62. Love MI, Huber W, Anders S. 2014. Moderated estimation of fold change and dispersion for RNA-Seq data with DESeq2. Genome Biol 15:550. https://doi.org/10.1186/s13059-014-0550-8
63. Maufrais C, de Oliveira L, Bastos RW, Moyrand F, Reis FCG, Valero C, Gimenez B, Josefowicz LJ, Goldman GH, Rodrigues ML, Janbon G. 2021. Population genomic analysis of *Cryptococcus* Brazilian isolates reveals an African type subclade distribution. G3 (Bethesda) 11:jkab107. https://doi.org/10.1093/g3journal/jkab107
64. Li Heng, Birol I. 2018. Minimap2: pairwise alignment for nucleotide sequences. Bioinformatics 34:3094–3100. https://doi.org/10.1093/bioinformatics/bty191
65. Li H, Handsaker B, Wysoker A, Fennell T, Ruan J, Homer N, Marth G, Abecasis G, Durbin R, 1000 Genome Project Data Processing Subgroup. 2009. The sequence alignment/map format and SAMtools. Bioinformatics 25:2078–2079. https://doi.org/10.1093/bioinformatics/btp352
66. Rosenberg A, Ene IV, Bibi M, Zakin S, Segal ES, Ziv N, Dahan AM, Colombo AL, Bennett RJ, Berman J. 2018. Antifungal tolerance is a subpopulation effect distinct from resistance and is associated with persistent candidemia. Nat Commun 9:2470. https://doi.org/10.1038/s41467-018-04926-x